Solid Freeform Fabrication 2024: Proceedings of the 35th Annual International Solid Freeform Fabrication Symposium – An Additive Manufacturing Conference
Reviewed Paper

Spreadability of Raw Sand in Binder Jet Additive Manufacturing: Examining Feasibility Using Numerical Methods

Ibrahim Al Qabani[1], Karin Goldberg[2], Drew Snelling[3], Hossein Taheri[3], Rafael Quirino[4], S. M. Thompson[*1]

[1] Department of Mechanical & Aerospace Engineering, University of Missouri, Columbia, MO 65211, United States of America.
[2] Department of Geology, Kansas State University, Manhattan, KS 66502, United States of America.
[3] Department of Manufacturing Engineering, Georgia Southern University, Statesboro, GA 30460, United States of America.
[4] Chemistry Department, Georgia Southern University, Statesboro, GA 30460, United States of America.

*Corresponding author: smthompson@missouri.edu

Abstract

In binder jet additive manufacturing (BJAM), uniformity and density of the powder layer impact green part quality. This study investigates the printability of unrefined sand using counter-roller spreading. Altair EDEM, a high-performance software powered by the Discrete Element Method (DEM), was used to simulate the BJAM process to evaluate powder bed homogeneity and density under various operating conditions, including roller rotational speed, traverse speed, powder layer thickness, and roller diameter. Utilizing high-performance computing (HPC) and graphics processing unit (GPU) clusters, time-efficient, and more realistic, simulations were performed simulating 300,000 grains. Detailed DEM simulations were executed by reconstructing representative particle shapes using two-dimensional images obtained using particle characterization equipment. The results highlight roller velocity and powder layer thickness as key determinants of sand spreadability. Optimal powder bed density (PBD) was achieved at a roller velocity of 20 mm/s with minimal deviation. A layer thickness exceeding 200 micrometers was found to prevent jamming and void formation, while percolation led to size segregation. The findings indicate that producing uniform and dense layers of unrefined sand is feasible but may incur trade-offs in print resolution and increased printing times. This work contributes to the advancement of sustainable and/or remote BJAM technologies, ensuring progress in both environmental sustainability and accessibility.

Keywords: DEM (Discrete Element Method); additive manufacturing (AM); powder bed density (PBD); fraction standard deviation (FSD).

1. Introduction

Additive manufacturing (AM), or 3D printing, is the process of fabricating objects one layer at a time [1]. It has proven to be a game changer for various industries, particularly the healthcare, automotive, aerospace, and defense industries. Fabricating objects one layer at a time allows for greater design freedom, greater complexity, and less overall waste [1]. It can create

lighter, better-performing, greener, and potentially cheaper products. There are seven different types of AM processes: material extrusion (MEX), sheet lamination (SHL), binder jetting (BJ), material jetting (MJT), directed energy deposition (DED), powder bed fusion (PBF), and vat photopolymerization (VPP) [1].

This research focuses on BJ for 3D printing raw earth materials. BJ is an AM technology that uses a drop-on-demand (DOD) printhead to selectively deposit a liquid binding agent onto a thin layer of powder particles. The binder bonds the powder particles in the selected areas to form a solid, three-dimensional part one layer at a time [2]. The process is repeated layer by layer until the final part is completed. The powder feedstock and building platform are linked to vertical pistons moving along the z axes, while the inkjet printhead traverses horizontally in the x and y axes. BJ systems can process a wide range of powder-based materials, such as metal, sand, ceramics, or composites, to fabricate solid parts. This investigation focuses on the feasibility of adopting unrefined, locally sourced raw earth sediments for BJ technology by examining the layer deposition stage, which is a vital stage in the printing process.

In BJ AM, the uniformity and packing density of the deposited powder layer affect the green density of the fabricated part [2], [3]. By optimizing the spreading process's input parameters, such as the system's operating conditions, a dense, homogenous spread layer can be produced [2], [3]. The discrete element method (DEM) is a numerical tool for solving engineering problems in granular flows, making it an ideal tool for computing the motion of sand grains [4]. Many studies have implemented this numerical technique to study powder spreading dynamics in AM technologies. Zhang et al. conducted a DEM on the effect of roller-spreading parameters on PBD in AM [5], focusing on Al_2O_3 ceramic powders composed of spherical particles with various size distributions. They considered parameters such as particle size, density, shear modulus, and Poisson's ratio. The study found that increasing the roller's translational velocity resulted in fewer particles in the powder layer zone, leading to low PBD [5]. Layer thickness was also discovered to be the most influential factor in PBD [5]. Nan, Pasha, and Ghadiri conducted a numerical simulation of particle flow and segregation during the roller spreading process in AM [6], focusing on gas-atomized 316L stainless steel particles with irregular shapes. The study compared cylindrical rollers and blade spreaders. Results showed that rollers outperformed blade spreaders in particle volume at low rotational speeds and equal translational velocities [6]. Additionally, larger particles exhibited more extensive segregation and were more sensitive to gap height and roller rotation speed [6]. This study aims to investigate the spreading and dynamic flow behavior of unrefined, poorly sorted sand grains during BJAM using EDEM. The PBD and uniformity of the spread layer are analyzed according to the mitigated process parameters.

2. Discrete Element Method (DEM)

Altair EDEM is used to model the powder spreading process in AM at the particle scale. The influence of the spreading input parameters (roller rotational speed, roller traverse speed, roller diameter, and layer thickness) on the behavior of the powder flow during layer spreading is investigated. Using numerical integration, the numerical approach solves Newton's equations of motion to compute particle accelerations, velocities, and positions [7]. In a granular flow, each particle has six degrees of freedom. This results in two types of motion: translational and rotational [7]. The translational motion is calculated using Eq. (1):

$$m\frac{\mathrm{d}v}{\mathrm{d}t} = F_g + F_c + F_{nc} \tag{1}$$

Here v is the translational velocity of the particle, m is the mass of the particle, F_g is the resultant gravitational force acting on the particle, F_c and F_{nc} are the resultant contact noncontact forces between the particles and surrounding particles and walls.

The rotational motion is calculated using the following equation:

$$I\frac{\mathrm{d}\omega}{\mathrm{d}t} = M \tag{2}$$

Here, I is the moment of inertia, ω is the angular velocity, M is the resultant contact torque acting on the particle, t is time.

3. Raw Materials

In this study, unrefined, locally sourced sand is used as feedstock material. It is collected in the Gypsum Hills, along Highway 281 north of Medicine Lodge in Barber County, KS. It is a very fine, fairly sorted sand made of quartz and red shales, gypsum, and mica. The Morphologi G3 equipment was used to measure the physical properties of 10,000 grains taken from the sand sample. The equipment unveiled a particle size distribution ranging from 2.18 to 270.32 micrometers, with an average grain size of 15.34 micrometers. The number-based equivalent circle diameters D_{10}, D_{50}, and D_{90} are 3.45 μm, 9.37 μm, and 34.70 μm, respectively.

4. Particle Morphology

Particle shapes significantly influence powder flow properties in AM [8]. Spherical particles are preferred for their superior flow characteristics, due to minimal friction and reduced interlocking [2]. However, unrefined sand, a heterogeneous mixture of rock and granular materials, contains grains with diverse shapes ranging from spherical to angular [9].

For computational efficiency, simple spherical particles are preferred because they simplify contact detection during simulations [7]. However, many applications require the modeling of irregular particle shapes. The Altair EDEM multi-sphere method allows the manual modeling of these irregular shapes by approximating them with numerous overlapping or contacting spheres with fixed centers. This method balances computational efficiency with the need for accurate geometric representation [7].

The Malvern Instruments Morphologi G3 provides precise PSD analysis and investigates the morphological characteristics of individual particles using high-resolution 2D imaging. The system categorizes particles based on three key factors: circularity, convexity, and elongation. Circularity, ranging from 0 to 1, measures the roundness of a particle, with values closer to 1 indicating more circular shapes. Convexity measures surface roughness, where higher values indicate smoother surfaces. Elongation, also ranging from 0 to 1, describes the aspect ratio of a particle's projection, with values closer to 1 representing more elongated shapes.

In this study, a sand sample containing 10,000 grains was analyzed. To manage computational resources, 25 distinct grain shapes were selected for EDEM simulations after a thorough examination of 2D images, ensuring all shape categories—angular, well-rounded, sub-rounded, sub-angular, and elongated particles—were represented [9], [20]. These particles were then manually constructed in EDEM using visual analysis and particle size data, with the software allowing for the combination of spheres to accurately represent the particles' edges and

imperfections. Fig. 1 illustrates the 2D images of the particles and their reconstructed counterparts in the EDEM software.

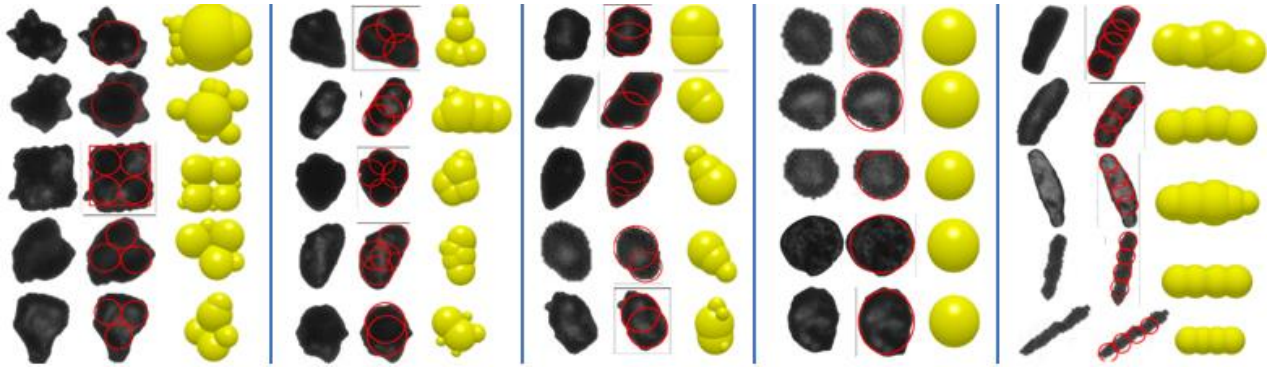

Fig. 1: Particle shapes used in DEM simulations.

As shown in Fig. 1, the particles are divided into five columns; each column contains an image of the reconstructed particles in the EDEM software. The far left of each column displays the 2D images of the selected particles. The middle row highlights the particle's basic structure or body, which represents the major sphere or spheres that will serve as the particle's main body. This method has advantages such as computing efficiency and low setup expenses.

5. Challenges

Achieving a high degree of homogeneity and packing density in the spread layer in binder jet applications is crucial and difficult [10]. To achieve such a layer, proper powder flowability is required. That being stated, it is concerning to learn that powder morphology governs the processability of BJ applications [11]. In fact, particle characteristics directly affect processing parameters in BJ [11].

Both process and material-related parameters contribute to the structural integrity and quality of printed parts [11]. In terms of material-related parameters, powder size directly affects flowability, with high packing density proportional to the particle size distribution (PSD) [11]. Coarse particles tend to flow better than fine particles due to reduced attractive forces like Van Der Waals, electrostatics, and cohesion [2]. Additionally, the grain's morphological properties influence the packing density of the powder bed [2]. For process-related parameters, inadequate spread speeds result in a heterogeneous spread layer with large porosity [10], and low speeds significantly increase printing time. Therefore, various simulations are needed to find the optimal speed balancing layer quality and printing time. Layer thickness, the height of the powder bed along the Z-axis, is governed by powder size [2]. Small thicknesses can reduce PBD due to particle jamming, while large thicknesses negatively impact dimensional accuracy and binder saturation [2].

Simulation Set-Up. The spreading process must be investigated for worst-case scenarios, meaning the system must process all grain shapes and sizes. To demonstrate the effectiveness of optimized operating parameters, they must be tested on realistic grain shapes. Creating 3D models of all grain shapes is unfeasible, so a suitable number must be chosen for simulation. This raises questions about the adequacy of the chosen number of grain shapes. For example, simulating 25 different shapes might seem reasonable, but if insufficient, it could lead to false forecasts and less effective spreading in real-world applications. To validate the selection of 25 grain shapes, the

simulation must ensure the particle shapes account for all sand classifications, from well-rounded to angular. Advanced instruments are needed to characterize sediment properties and composition in detail. Manually reconstructing particle shapes in EDEM based on visual analysis requires precise adjustments of numerous spheres, relying on assumptions about the degree of accuracy. More spheres per particle demand more computation time, impacting computational performance and precision. EDEM's high-performance software requires extreme computational power. Testing a well-sorted sample with well-rounded grains is already computationally intensive; simulating a poorly sorted sample with varied grain shapes is even more demanding. Generating and simulating hundreds of thousands of grains is time-consuming, and changing operating parameters and rerunning simulations can be exhausting.

Binder Saturation. The migration of the binder in the powder bed is not the primary focus of this study, but a brief discussion on binder saturation challenges is relevant. Binder saturation is influenced by the uniformity and packing density of the deposited layer. According to the literature [12], the permeability of a sand sample is primarily affected by grain size, morphology, and bed compactness. Since the raw material characteristics are beyond this study's control, adjusting process parameters to account for sand sample irregularities is challenging. Angular particles can hinder powder flowability, agglomerate in the powder bed, and cause void defects during spreading, leading to a heterogeneous powder distribution [2]. This distribution can create pathways and barriers that disrupt droplet penetration. Additionally, agglomerated fine particles form macro-voids, obstructing the binder's penetration path and significantly increasing penetration time [2].

According to the aforementioned challenges, it is clear that the physical characteristics of the raw material govern the process-related parameters. The focus is to explore the printability of unrefined sand. As a result, the investigation's sole controllable variables are process-related parameters. While the raw material's properties remain constant, adjustments to process parameters are made based on the quality of the deposited layers. With so few alternatives, extensive simulations are necessary. Additionally, each process parameter requires a separate investigation, as minor adjustments can lead to numerous possibilities. The complex and diverse physical properties of sand amplify the challenge of adjusting process-related parameters.

6. Simulation Setup

Roller Spreading Input Parameters. Table 1 summarizes the spreading parameters that will be modified after each simulation run. Keep in mind that the gap height is predetermined because this particular BJ configuration is based on a stationary powder bed; in other words, the build platform will drop down by the prescribed layer thickness after each layer is distributed. Essentially, the predetermined gap height guarantees that the spreader does not touch the surface during movement, preventing damage and maintaining uniform deposition. The simulation includes a cylindrical counter roller, a powder bed, and a build platform, as shown in Fig. 2. The counter roller serves as a spreading device, rotating counterclockwise as it moves across the powder bed and platform in linear motion. The roller moves at speed V_s while it rotates in the counterclockwise direction at speed ω to transport the particles from the powder bed to the build platform, forming a layer of spread powder.

Table 1: Spreading parameters.

Parameters	***Values***

Roller's traverse speed V_s (mm/s)	20, 40, 60, 80, 100, 120, 140, 160, 180, 200
Roller's rotational velocity ω (rpm)	100, 120, 140, 160, 180, 200, 220, 240, 260, 280
Roller's diameter D (μm)	2, 3, 4, 5
Powder layer thickness H (μm)	40, 60, 80, 100, 120, 140, 160, 180, 200, 220
Gap height δ (μm)	10

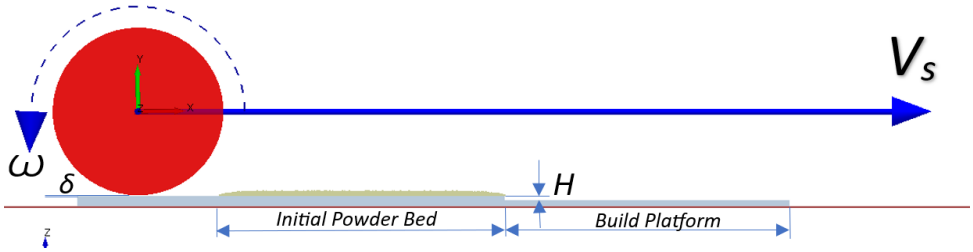

Fig. 2: Process parameters in the powder spreading simulation setup.

Bulk Material Properties. To accurately simulate particle motion and interaction via DEM, input parameters for the material properties of the powder particles and walls are required. These properties can be sourced from previous studies on similar materials to avoid the high cost of experimental determination. Particle-wall interactions represent the contact between sand grains and the environment, such as the build platform or roller.

Table 2: Material properties.

Parameters	***Value***	***Units***
Solid Density (ρ)	1600	kg/m^3
Youngs Modulus (E)	90.1	GPa
Poisson's Ratio (η)	0.32	
Coefficient of Restitution (Particle-Particle)	0.88	
Coefficient of Static Friction (Particle-Particle)	0.24	
Coefficient of Rolling Friction (Particle-Particle)	0.75	
Coefficient of Restitution (Particle-Wall)	0.68	
Coefficient of Static Friction (Particle-Wall)	0.50	
Coefficient of Rolling Friction (Particle-Wall)	0.65	

8. Characteristics of the Spread Layer

PBD of the dispensed layer must be adequate for optimum binding. Hence, the PBD is investigated and the adjustments to the operating parameters are made accordingly. Results from each layer deposition simulation are compared based on their PBD values. Parameters resulting in optimal PBD are prioritized. Second, the segregation of the powder layer is examined for each simulation run. The segregation of the density, particle size, and morphology will narrate how uneven the powder layer is. In powder-based AM, particle size segregation is undesirable, especially in materials with wide size distributions [1]. Literature [2] states that percolation effects in such powders lead to segregation, creating larger vacancies and altering PBD. Fine particles move faster than coarse ones, leading to separation and additional voids.

Powder Bed Density (PBD). PBD can be measured by examining a defined enclosure within the deposited layer. It is advised that one investigates multiple locations across the powder bed to analyze the densities uniformity [10]. PBD is determined by computing the material density within a confined area. It quantifies the amount of material present per unit volume, typically expressed as [13]:

$$\text{Apparent density of each grid} = \emptyset_i = \frac{\sum_{i=1}^{N} m_i}{V_i} \tag{3}$$

where, m_i = Particle mass of grid i, and V_{Total} = Volume of grid i.

The values for m_i can be directly obtained from the EDEM simulation results. Generally, in the context of AM, the higher the PBD, the better [14]. To consider all grids, the overall average PBD will be determined by dividing the sum of the PBD for each grid by the number of grids (N), which is represented as:

$$\overline{\emptyset} = \frac{\sum_{j=1}^{N} \emptyset_i}{N} \tag{4}$$

Where N is the total number of grids, and $\emptyset_i$ is the PBD for each grid.

Segregation. In 3D printing, particle segregation refers to the uneven distribution of particle size, shape, or other physical properties across the powder bed [15]. Segregation occurs when the PSD of the deposited layer differs from the initial powder bed PSD [15]. Powder beds with a wide PSD are more prone to segregation, which is common in raw earth materials. While controlling material properties is not an option, appropriate process parameters, such as spreading speed and layer thickness, can mitigate segregation [2], [14], [15].

The fraction standard deviation (FSD) is used to determine segregation in the powder bed. A low FSD indicates a more homogeneous PSD. The formula for calculating the standard deviation of the PBD across the spread layer is provided in [14], [15].

$$\sigma_{\overline{\emptyset}} = \sqrt{\frac{1}{N-1}\sum_{i=1}^{N}\left(\emptyset_i - \overline{\emptyset}\right)^2} \tag{5}$$

where N = Number of defined regions, $\emptyset_i$ = PBD at the ith location, $\overline{\emptyset}$ = average PBD.

To apply equations 3 & 5 above, the powder bed deposited on the substrate will be divided into grids that stretch along the length and width of the substrate. The thickness of the grids corresponds to the layers thickness, which is along the z axes.

9. Results

Particle Properties & Layer Characteristics – Powder Segregation. Interestingly, the findings support the literature's claim that powdered materials with a wide PSD will experience percolation during spreading, resulting in powder demixing and segregation, with finer fractions on the bottom and coarser fractions on top [2], [16]. Gravity influences the process by causing tiny particles to seep downward while bigger particles remain stagnant [2]. Percolation involves particles passing through temporary voids or channels within the powder packing. Finer particles move downward under gravity, forming routes for other particles to follow, resulting in size

segregation [16]. This percolation segregation process mainly occurs within the dynamic powder avalanching during spreading. For example, Fig. 3 shows that the fine particles are primarily concentrated in the bottom fraction of the layer and powder heap, while coarse particles are found in the top fractions of both the heap and the layer.

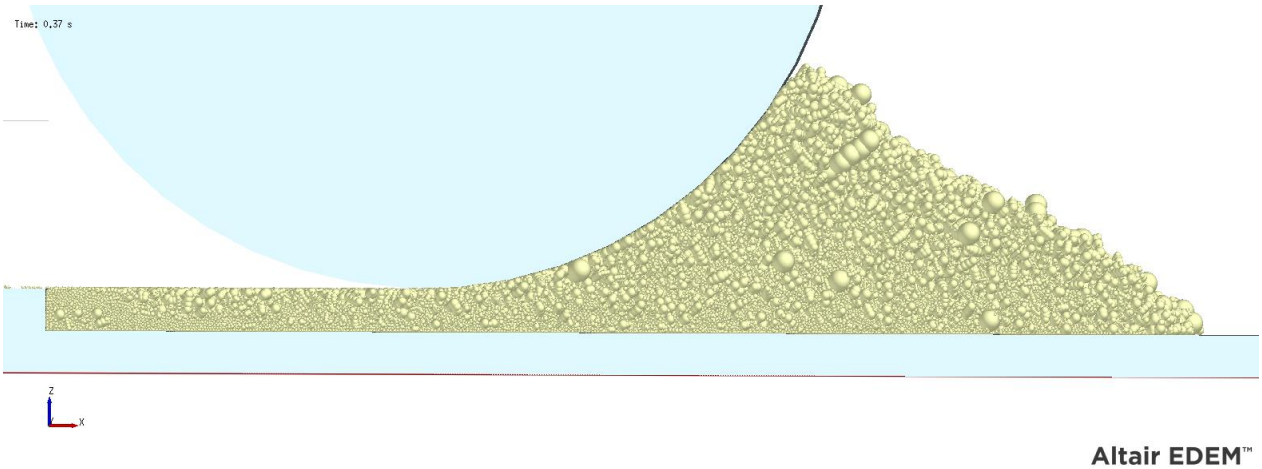

Fig. 3: Percolation segregation occurs when powder avalanches during spread.

The influence of the layer thickness on the spread layer packing density. In BJ, layer thickness is the height of the powder bed along the z-direction, typically ranging from 15 to 300 micrometers [2], [21]. For example, the Voxeljet VXC800 machine uses layer thicknesses between 150 to 400 microns for sand-casting [21]. Some studies recommend using a layer thickness 2 to 3 times the powder size or even larger than the largest particle size [2], [22].

Layer thickness, governed by desired printing resolution and PBD, affects packing density and binder saturation, which in turn influences the strength and surface quality of printed parts [23]. Optimizing binder saturation requires monitoring the homogeneity of the deposited layer at various thicknesses [23]. Research shows that layer thickness and binder saturation significantly impact the strength, integrity, and dimensional accuracy of printed parts [80]. Additionally, layer thickness, along with particle size, affects the surface finish [2].

Figure 4 illustrates that the fraction standard deviation (FSD) decreases with increasing powder layer thickness, with a notable drop between 120 and 180 micrometers, and a gradual reduction beyond that. The uniformity of the deposited layer is optimal at 120 micrometers, and thicknesses above 180 micrometers help maintain this uniformity. Figure 4b shows that PBD increases with layer thickness; from 40 to 120 micrometers, it rises significantly in a linear fashion but increases minimally from 120 to 220 micrometers. Optimal PBD is achieved at layer thicknesses of 120 micrometers or higher, with 220 micrometers being ideal.

In narrow gaps, particle jamming can reduce PBD. Larger particles may block smaller particles, causing accumulation and obstruction [21]. Irregularly shaped particles are more likely to interlock, leading to compression and pushing particles out of the build platform, resulting in large voids in the deposited layer.

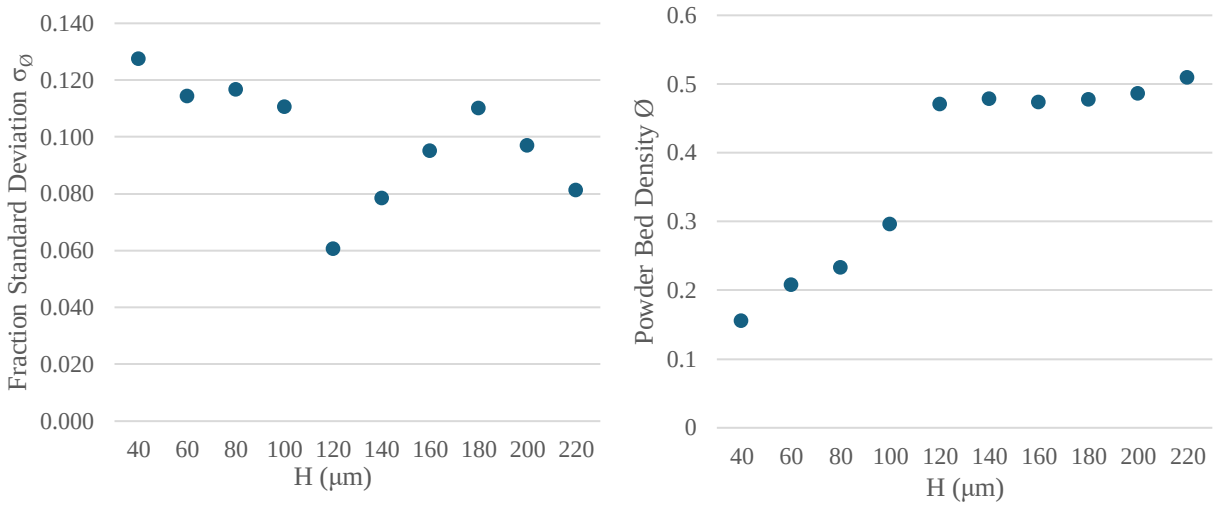

(a) FSD (b) PBD

Fig. 4: Influence of layer thickness with D = 4 mm, ω = 200 rpm, and V_s = 20 mm/s.

The influence of the roller traverse speed on the spread layer packing density. The traverse speed of a roller is the rate at which it moves across the build platform while rotating. This speed significantly influences PBD and homogeneity [2, 17]. Studies highlight that roller traverse speeds exceeding 40 mm/s can lead to an uneven powder bed, resulting in macro-voids in subsequent layers [2], [13], [14], [17]. Lower speeds are generally preferred for consistent spreading and improved packing of finer particles ($\leq$ 2.5 µm), despite potentially increasing overall printing time [2]. Conversely, higher speeds may be suitable for coarse particles [2]. An experimental investigation explored traverse speeds ranging from 6 mm/s to 14 mm/s, with specific levels set at 6 mm/s, 10 mm/s, and 14 mm/s. The findings revealed that optimal uniformity was achieved at 6mm/s, albeit with a notable increase in printing time [18]. In this experiment, the roller traverse speed ranged from 20 mm/s to 200 mm/s in 20 mm/s increments. The results align with previous findings, showing that PBD decreases with higher traverse speeds while FSD increases. Therefore, optimal layer spreading is achieved at lower traverse speeds, specifically those below 40 mm/s. Traverse speed emerges as a critical factor, as both PBD and FSD exhibit significant variations in response to changes in traverse speed. The PBD follows a linear trend, consistent with findings reported by Zhang et al. [13]. Notably, the PBD reaches its peak, just below 0.5, at a traverse speed of 20 mm/s.

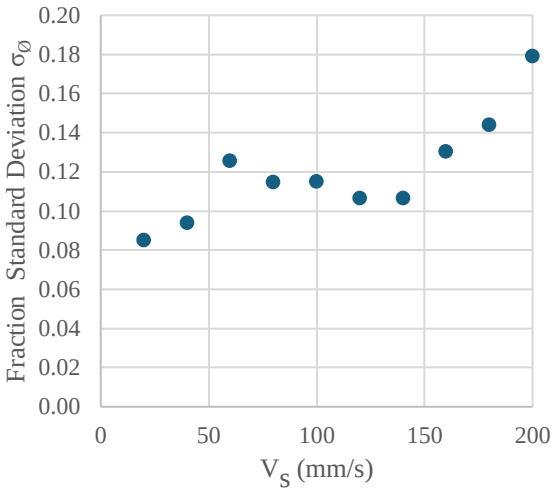

(a) FSD

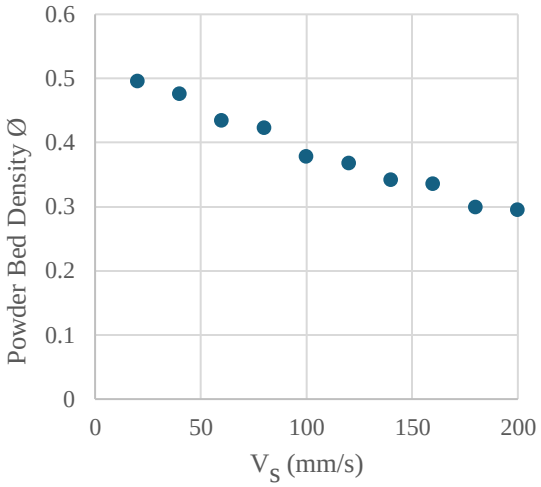

(b) PBD

Fig. 5: Influence of roller's traverse speed with D = 4 mm, ω = 200 rpm, and H =200 µm.

Conversely, the lowest PBD, slightly below 0.3, is observed at a traverse speed of 200 mm/s. On the other hand, FSD is attained at the lowest traverse speed, slightly above 0.08. This relationship changes as the traverse speed increases, with the highest FSD achieved at the maximum traverse speed.

The influence of the roller diameter on the spread layer packing density. Adjustments to the roller diameter did not cause significant changes in both PBD and FSD. Specifically, PBD fluctuated within a narrow range of 0.45 to 0.49, indicating negligible change. In contrast, FSD varied between 0.07 and 0.1, showing a slightly more significant impact. Ultimately, roller diameter is not as influential compared to other parameters. However, it is noteworthy that a 4 mm diameter roller resulted in the highest FSD, which is balanced by also achieving the highest PBD.

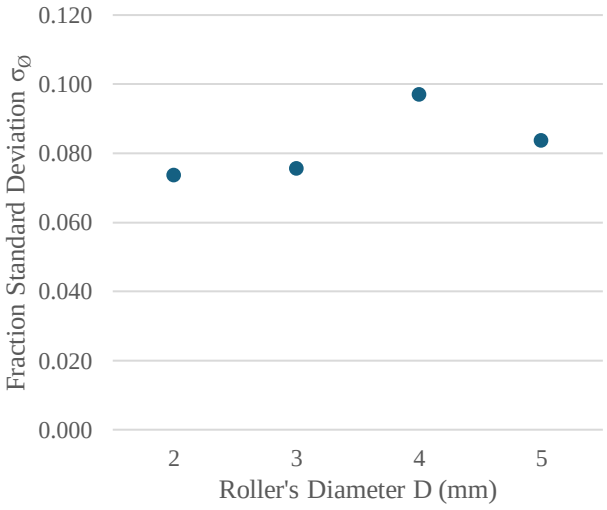

(a) FSD

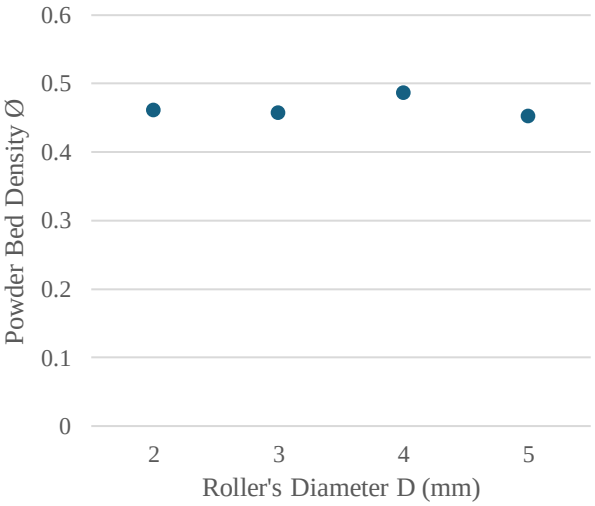

(b) PBD

Fig. 6: The influence of roller's diameter when V_s = 20 mm/s, ω = 200 rpm, and H =200 µm.

The influence of the roller rotational speed on the spread layer packing density. Rotational speed, or angular velocity, is typically measured in rad/s or rpm. For instance, the M-Flex ExOne printer uses a roller rotating at 250 rpm, while the ZPrinter 310 Plus Z Corp. operates at 75 or 145 rpm [2]. Zhang et al. investigated the impact of roller-spreading parameters on PBD, testing speeds from 40 to 320 rpm. Their findings suggested that rotational speed had no significant effect on PBD, though a higher ω could improve poor flowability [19]. As shown in Fig. 7, rotational speed has minimal effects on both PBD and FSD. PBD remains constant until it slightly drops at speeds above 220 rpm. FSD oscillates between 0.060 and 0.100, with minimal influence from rotational speed. From the data, 140 rpm is adequate as it results in low FSD and high PBD.

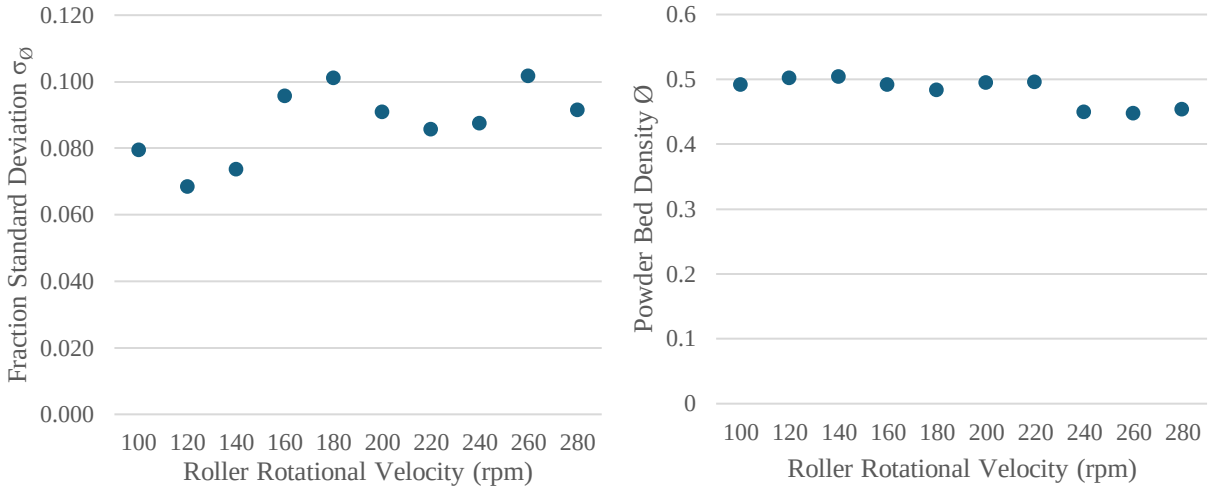

(a) FSD (b) PBD

Fig. 7: The influence of roller's traverse speed when V_s = 20 mm/s, D = 4 mm, and H =200 µm.

7. Conclusions

In this study, the DEM was used to simulate the spreading of unrefined sand using a counter-roller. The deposited layer was divided into forty grids to analyze PBD and FSD. The effects of powder spreading parameters, including translational velocity V_s, roller rotational speed ω, roller diameter D, and layer thickness H, are examined based on PBD and FSD. The goal was to investigate the feasibility of adapting unrefined sediments to this specific spreading technique. Key findings include:

1. Translational Speed: PBD constantly decreased with increasing roller translational speeds, indicating that lower translational velocities are recommended for high PBD in deposited layers. The optimal translational velocity was found to be 20 mm/s, resulting in the highest PBD and sufficiently low FSD.
2. Layer Thickness: Small layer thicknesses are not recommended as they result in inadequate PBD due to particle jamming during powder flowability. When the layer thickness is below 120 µm, the spread layer contains void spaces or empty patches due to inadequate powder flow through the gap between the build platform and the recoating mechanism (roller). Larger particles obstruct the flow, leading to uneven layers and poor packing density.
3. Rotational Speed: The rotational speed had minimal effect on PBD, remaining constant across settings, with 120 rpm being optimal.

4. Percolation: Simulations indicated significant percolation during spreading, leading to powder demixing and segregation, with finer fractions at the bottom and coarser fractions on top, observed under all process parameter adjustments.

Overall, it is feasible to adapt unrefined sediments to BJ systems utilizing counter-rollers, but this requires very low translational velocities and larger layer thicknesses. This adaptation comes at the cost of longer overall printing times and reduced printing resolution. In future work, industrial 3D scanning will be used to create 3D images of grains and produce STL files, which can be directly uploaded into Altair EDEM software. Altair EDEM will then construct an identical grain form by combining smaller spherical particles and adjusting their positions and sizes to match the sand grain's shape. This method will provide more accurate results compared to manually reconstructing grains from 2D images, which can introduce imperfections.

Acknowledgement

This material is based upon work supported by the National Science Foundation under Award #2423166.

References

[1] Gibson, I., Rosen, D. W., Stucker, B., Khorasani, M., Rosen, D., Stucker, B., & Khorasani, M. (2021). Additive manufacturing technologies (Vol. 17, pp. 160-186). Cham, Switzerland: Springer.

[2] Mostafaei, A., Elliott, A.M., Barnes, J.E., Li, F., Tan, W., Cramer, C.L., Nandwana, P. and Chmielus, M., 2021. Binder jet 3D printing—Process parameters, materials, properties, modeling, and challenges. *Progress in Materials Science*, *119*, p.100707.

[3] Miyanaji, H. (2018). Binder Jetting Additive Manufacturing Process Fundamentals and the Resultant Influences on Part Quality. https://doi.org/10.18297/etd/3058

[4] Fouda, Y.M. and Bayly, A.E., 2020. A DEM study of powder spreading in additive layer manufacturing. Granular Matter, 22(1), p.10.

[5] Zhang, J., Tan, Y., Bao, T., Xu, Y., Xiao, X. and Jiang, S., 2020. Discrete element simulation of the effect of roller-spreading parameters on powder-bed density in additive manufacturing. *Materials*, *13*(10), p.2285.

[6] Nan, W., Pasha, M. and Ghadiri, M., 2020. Numerical simulation of particle flow and segregation during roller spreading process in additive manufacturing. Powder Technology, 364, pp.811-821.

[7] Theoretical background behind the Discrete Element Method (DEM) http://www.altair.com/edem

[8] Nasato, D.S. and Pöschel, T., 2020. Influence of particle shape in additive manufacturing: Discrete element simulations of polyamide 11 and polyamide 12. *Additive Manufacturing*, *36*, p.101421.

[9] Li, L. and Iskander, M., 2021. Evaluation of roundness parameters in use for sand. *Journal of Geotechnical and Geoenvironmental Engineering*, *147*(9), p.04021081.

[10] Miyanaji, H. (2018). Binder Jetting Additive Manufacturing Process Fundamentals and the Resultant Influences on Part Quality. https://doi.org/10.18297/etd/3058

[11] Dini, F., Ghaffari, S.A., Jafar, J., Hamidreza, R. and Marjan, S., 2020. A review of binder jet process parameters; powder, binder, printing and sintering condition. *Metal Powder Report*, *75*(2), pp.95-100.

[12] Coniglio, N., Sivarupan, T. and El Mansori, M., 2018. Investigation of process parameter effect on anisotropic properties of 3D printed sand molds. The International Journal of Advanced Manufacturing Technology, 94, pp.2175-2185.

[13] Zhang, J., Tan, Y., Xiao, X. and Jiang, S., 2022. Comparison of roller-spreading and blade-spreading processes in powder-bed additive manufacturing by DEM simulations. *Particuology*, *66*, pp.48-58.

[14] Xiao, X., Jin, Y., Tan, Y., Gao, W., Jiang, S., Liu, S. and Chen, M., 2022. Investigation of the Effects of Roller Spreading Parameters on Powder Bed Quality in Selective Laser Sintering. *Materials*, *15*(11), p.3849.

[15] Nan, W., Pasha, M. and Ghadiri, M., 2020. Numerical simulation of particle flow and segregation during roller spreading process in additive manufacturing. Powder Technology, 364, pp.811-821.

[16] Capozzi, L.C., Sivo, A. and Bassini, E., 2022. Powder spreading and spreadability in the additive manufacturing of metallic materials: a critical review. *Journal of Materials Processing Technology*, *308*, p.117706.

[17] Mussatto, A., Groarke, R., O'Neill, A., Obeidi, M.A., Delaure, Y. and Brabazon, D., 2021. Influences of powder morphology and spreading parameters on the powder bed topography uniformity in powder bed fusion metal additive manufacturing. *Additive Manufacturing*, *38*, p.101807.

[18] Shrestha, S. and Manogharan, G., 2017. Optimization of binder jetting using Taguchi method. Jom, 69, pp.491-497.

[19] Zhang, J., Tan, Y., Bao, T., Xu, Y., Xiao, X. and Jiang, S., 2020. Discrete element simulation of the effect of roller-spreading parameters on powder-bed density in additive manufacturing. *Materials*, *13*(10), p.2285.

[20] Blott, S.J. and Pye, K., 2008. Particle shape: a review and new methods of characterization and classification. Sedimentology, 55(1), pp.31-63.

[21] Gibson, I., Rosen, D.W., Stucker, B., Khorasani, M., Rosen, D., Stucker, B. and Khorasani, M., 2021. *Additive manufacturing technologies* (Vol. 17, pp. 160-186). Cham, Switzerland: Springer.

[22] Simchi, A., 2004. The role of particle size on the laser sintering of iron powder. *Metallurgical and Materials Transactions B*, *35*, pp.937-948.

[23] Vaezi, M. and Chua, C.K., 2011. Effects of layer thickness and binder saturation level parameters on 3D printing process. *The International Journal of Advanced Manufacturing Technology*, *53*, pp.275-284.